Ultrafast electron dynamics in metals: Real-time analysis of a reflected light field using photoelectrons

U. Bovensiepen,[1,*] S. Declair,[2] M. Lisowski,[1,†] P. A. Loukakos,[1,‡] A. Hotzel,[1] M. Richter,[2] A. Knorr,[2] and M. Wolf[1,3]
[1]*Fachbereich Physik, Freie Universität Berlin, Arnimallee 14, 14195 Berlin, Germany*
[2]*Institut für Theoretische Physik, Technische Universität Berlin, 10623 Berlin, Germany*
[3]*Fritz-Haber-Institut der MPG, Faradayweg 4-6, 14195 Berlin, Germany*
(Received 3 October 2008; published 20 January 2009)

We propose an approach to address ultrafast charge-carrier dynamics of metals by analyzing the momentum change in photoelectrons interacting with a transient optical grating at a metal surface. Photoelectrons are excited by an ultraviolet femtosecond laser pulse which precedes an infrared pulse setting up the transient grating. We measure the kinetic energy of the photoelectrons which are accelerated by the grating's ponderomotive potential and thus sample the respective electric field. The method is capable to access phase and amplitude differences between the incoming and the reflected light fields. The latter is determined by the response of the conduction-band electrons to the light field. We report on a demonstration of such an experimental scheme using a Gd(0001) surface and calculate the reflected field by a simplified transport equation. We derive a method to determine the average electron-scattering rate and study the time-dependent evolution of amplitude and phase of the reflected electric field including memory effects in the optically induced polarization dynamics. Finally, we discuss the required steps of this approach to probe ultrafast dynamics in metals experimentally.

DOI: 10.1103/PhysRevB.79.045415 PACS number(s): 78.47.−p, 52.35.Mw, 79.60.Bm

I. INTRODUCTION

Investigations of the dynamical response in time domain bear the potential to obtain insight into the time development of the underlying microscopic processes. Optical pump-probe experiments represent a well established approach to analyze the evolution of the perturbed system after an impulsive excitation as a function of time delay to a second pulse, which probes the corresponding transient state. The analysis of such transients is straight forward as long as coherence times are considerably shorter than the pulse duration and a simple rate equation analysis of the population dynamics is sufficient. In case of overlapping pulses or long coherence times the analysis is more demanding and requires a detailed modeling which includes a theoretical description of the polarization dynamics.[1,2] Depending on the system, various processes determine the optical response of the material such as molecular vibrations in solution[3,4] or proteins,[5] as well as electronic excitations of semiconductors,[6,7] electron-ion plasma collisions,[8,9] and electron collisions in metallic structures.[10]

Time-resolved experiments which address the problem of coherent polarization employ nonlinear methods[11,12] or interferometric approaches.[13] The required time resolution is on the order of the respective lifetime and decoherence time of the elementary excitation of interest. Typical time scales range from picoseconds to attoseconds for electronic transitions in semiconductor quantum well structures[6] in the infrared (IR) and in metallic structures in the visible and ultraviolet (UV) spectral regime.[10] In the following we focus on metals and their surfaces, at which electronic coherence times have been analyzed by time-resolved photoemission experiments[13–15] or nonlinear optics.[12] For further motivation a light field is considered which is incident on a metal surface and drives a collective excitation of the conduction electrons, i.e., plasmonic excitations.[16] Because typical dephasing and lifetimes for plasmons are in the subfemtosecond to femtosecond range, the electronic system is assumed to be excited by the light field on a subfemtosecond time scale. Owing to the plasma frequency, which is on the order of few eV, and the large bandwidth of the conduction-electron response, the plasmon coherence time is only of a few optical cycles.[17] Experiments that address this problem completely in the time domain would thus require attosecond time resolution. Attosecond time-resolved experiments have been pioneered by Krausz and co-workers[18–20] and were recently extended to metal surfaces.[21] However, complementary approaches to address ultrafast dephasing processes and high scattering rates in solids might be valuable because of the complexity of attosecond light sources[21] and the modeling required to analyze interferometric two-photon photoemission experiments.[13]

Here we present a transient grating approach that is sensitive to high electron-scattering rates $\Gamma > 1/\mathrm{fs}$ at metal surfaces using laser pulses with typically 100 fs duration. The optical grating is probed locally by a photoelectron as a function of distance from the metal surface. It is generated by reflection of an IR femtosecond laser pulse and the photoelectron is excited at the metal surface by a UV femtosecond laser pulse. The momentum of the photoelectron is modified by the ponderomotive potential ϕ_p of the transient grating. We measure the photoelectron's momentum change in photoemission as a function of position in the grating. Since the ponderomotive potential is determined by the superposition of incoming and reflected light fields, we have access to the response of the conduction electrons to the light field. This dynamics is described by a simplified transport equation. We derive an analysis of the average scattering rate and discuss the limit of a grating setup by a few-cycle optical pulses. Furthermore, we demonstrate that amplitude and phase of the

optical grating can be determined. Due to the optical cycle duration of the grating's frequency ($\lambda=830$ nm, $1/\nu=2.8$ fs) the scheme is sensitive for scattering rates $\Gamma > 1/\mathrm{fs}$.

Acceleration of free electrons has been achieved by optical transitions between continuum states. It can be driven by laser pulses and leads to above-threshold ionization which has been demonstrated for free atoms, molecules,[22] and solids.[23–25] Such transitions occur in the vicinity of a potential gradient because energy and momentum conservation prevent absorption of photons by free electrons in the vacuum. At sufficiently high laser intensity gas phase Auger[26] and photoelectron spectra[27] exhibit sidebands stemming from emission or absorption of laser photons. Sidebands have also been observed in photoemission from a Pt surface.[25] Using a few-cycle IR laser pulse for generation of attosecond extreme ultraviolet (XUV) pulses and for modification of the final state of a photoelectron excited by the XUV pulse, Krausz and co-workers[18–21] established a streaking technique facilitating attosecond (as) time resolution.

In electromagnetic fields the momentum $\mathbf{p}$ of photoelectrons is changed by the force of the instantaneous electric field acting on the electron $\mathbf{F}(\mathbf{r},t)=-e\mathbf{E}(\mathbf{r},t)$ which varies as a function of time with the high frequency ω of the IR wave. The corresponding electron motion is described by $\mathbf{r}=\mathbf{r}_0+\mathbf{r}_1$, with $\mathbf{r}_1$ oscillating at ω to account for the quiver motion and $\mathbf{r}_0$ the oscillation center. Expansion of the electric field to $\mathbf{E}(\mathbf{r})=\mathbf{E}(\mathbf{r}_0)+(\mathbf{r}_1\cdot\nabla_0)\mathbf{E}$ leads to a drift of $\mathbf{r}_0$ along a spatial field gradient. As the duration of the employed UV pulse exceeds an IR optical cycle and due to absence of carrier-envelope phase stabilization of the IR pulse our experiment is not sensitive to the quiver motion $\mathbf{r}_1$ and its effect on the kinetic energy is integrated out in time: $\phi_p \propto \langle E^2 \rangle$. Then, the equation of motion for a photoelectron with mass m is given in case of a standing optical wave by[28]

$$\frac{\partial^2 \mathbf{r}_0}{\partial t^2} = -\frac{e^2}{m^2\omega^2}\left\langle \nabla_0 \frac{E^2}{2} \right\rangle = -\nabla\phi_p. \tag{1}$$

As illustrated in Fig. 1(a), the spatial variation in ϕ_p along x accelerates an electron with initial momentum $p_x>0$ toward the nodes of the standing wave, i.e., the minima in ϕ_p. Thus an electron experiencing a positive gradient of ϕ_p is decelerated and is accelerated for $\partial\phi_p/\partial x<0$, respectively.

II. EXPERIMENTAL REALIZATION

In our experiment a standing wave is generated by reflection of an 830 nm femtosecond laser pulse at a single-crystal Gd(0001) metal surface under 45° angle of incidence. Figures 1(b)–1(d) depict the electric field energy density of the two-dimensional transient grating before, during, and after interference of the incident and reflected parts of the pulse. These laser pulses are delivered with a duration of 50 fs by an amplified Ti:sapphire laser system operating at 300 kHz repetition rate. A 3 μJ fraction is used to generate an *s*-polarized transient grating with a peak intensity of 50 GW/cm^2. Photoelectrons, which probe the transient grating, are excited at the metal surface in direct photoemission by a *p*-polarized 6 eV laser pulse with 90 fs duration. These

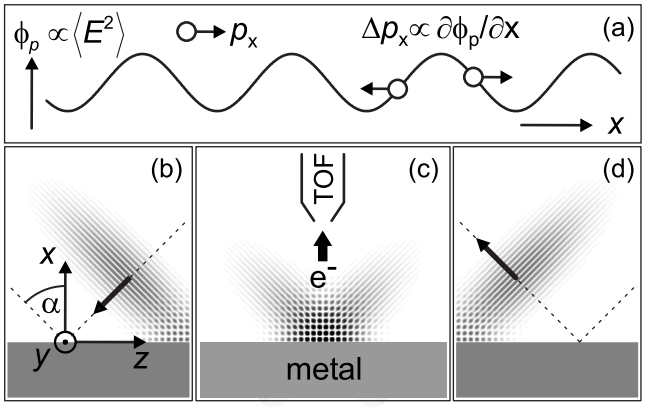

FIG. 1. (a) Acceleration of charged particles in the ponderomotive potential ϕ_p; (b)–(d) depict the experimental scheme of an infrared femtosecond laser pulse reflected at a metal surface. Incident and reflected parts overlap in space and form a two-dimensional transient grating. The electric field intensity is given by the gray scale. The intensity is maximum when the pulse center is located at the surface (c). Photoelectrons sense the standing wave and are analyzed in normal emission by an electron time-of-flight (TOF) spectrometer.

pulses are produced by quadrupling a 1 μJ portion of the IR pulse in two subsequent beta-barium borate nonlinear optical crystals and precede the IR pulse by a time delay Δt. For $\Delta t>0$ the UV pulse arrives before the IR pulse. The kinetic energy of photoelectrons is analyzed in normal emission by an electron time-of-flight spectrometer with an acceptance angle of $\pm 3°$ and energy resolution <20 meV [Fig. 1(c)].

The Gd(0001) surface was chosen due to its $5d_{z^2}$ surface state which provides a sharp feature in photoemission. Epitaxial Gd(0001) films of 10 nm thickness were grown *in situ* on a W(110) substrate under ultrahigh vacuum conditions.[29] The photoemission spectrum of the Gd(0001) surface, generated by the 6 eV laser pulses, is shown for a blocked IR pulse in Fig. 2, top. The high energy cutoff at a kinetic energy $E_{\mathrm{kin}}=2.68$ eV is determined by the Fermi energy E_F of the metal. Subtraction of the UV photon energy determines the work function to be 3.32 eV. The peak in the spectrum originates from the $5d_{z^2}$ surface state (majority-spin component) which has been studied extensively.[30–33] To monitor transient changes in the kinetic energy of the peak position, the high intensity part of the peak is fitted by a Gaussian as shown in the inset of Fig. 2. We do not intend a full lineshape analysis, which would require deconvolution of the laser-pulse bandwidth and the spectrometer resolution.[32,33] We rather aim at a precise analysis of the peak energy which will be modified by the transient optical grating.

After unblocking the IR pulse we observe as a function of delay between both laser pulses a variation in the photoemission spectrum. The bottom panel in Fig. 2 depicts E_{kin} of the surface-state peak as a function of delay. The peak energy oscillates with an amplitude of few meV, i.e., far below the UV laser-pulse bandwidth. Considering the velocity of an electron with $E_{\mathrm{kin}}=2.4463$ eV the observed frequency of $\Omega/2\pi=1.53$ THz corresponds to a period in space of 0.62 μm in front of the surface. We exclude that these os-

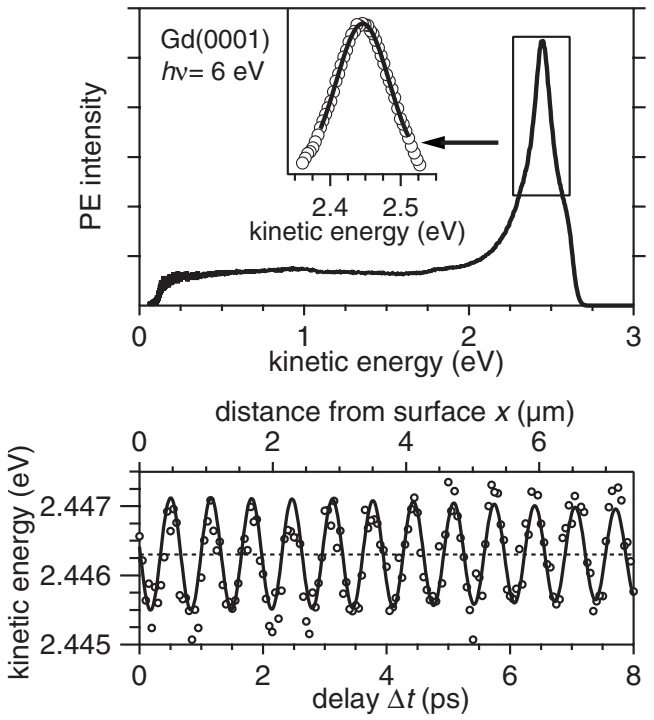

FIG. 2. Top: photoemission spectrum of Gd(0001) with $h\nu = 6$ eV taken at a temperature of 30 K. The inset includes a Gaussian fit of the surface-state peak. Bottom: circles indicate the kinetic energy of the peak measured for different delay, i.e., distance to the surface x (top or bottom axis). The solid line is calculated by Eq. (3). Errors bars are within the symbol size. The oscillations are observed up to 17 ps; however for clarity $\Delta t < 8$ ps is shown only.

cillations occur due to absorption of the IR laser pulse in Gd (discussed in Refs. 32 and 33) because at the arrival of the IR pulse the photoelectrons have already been emitted and have traveled in vacuum a distance x from the surface. We conclude that the oscillations in E_{kin} are induced by the transient IR grating and represent a variation in the photoelectron's final state in the continuum. This is shown by the following analysis. The energy modulation at Ω occurs due to a spatially varying field and is determined by the field periodicity along x and the electron momentum p_x.

To calculate the acceleration of the electron in the transient grating we integrate over the optical cycles of the IR pulse to average over the quiver motion according to Eq. (1). Due to the gradient $\nabla\phi_p$ an acceleration along x remains which is given by

$$\int F dt = \frac{e^2 \cos\alpha\sqrt{R}}{mc\omega} \int d\omega |\hat{E}^0|^2 \cos\psi. \tag{2}$$

Here, α denotes the angle of incidence, R the reflectivity, and ψ the phase change in the light field upon reflection at the metal surface.[34] We consider an s-polarized Gaussian laser pulse with the field maximum $\hat{E}^0 = \sqrt{8\pi\Phi\sigma/c}(2/\pi)^{1/4}$, where Φ is the incident fluence and σ defines the pulse duration [full width at half maximum (FWHM)] $\tau = \sigma\sqrt{8\ln 2}$. From the observed $\Delta E_{\mathrm{kin}}/E_{\mathrm{kin}}$ (Fig. 2) we determine $\Delta p_x/p_x = 3 \times 10^{-4}$ and p_x is approximated as a constant. Following Eq. (2) the kinetic-energy variation is given by

$$\Delta E_{\mathrm{kin}} = \frac{p_x}{m} \int F dt = \epsilon \cdot e^{-A - B\Delta t^2} \sin(\Omega \Delta t + \psi). \tag{3}$$

The energy variation is quantified by the amplitude $\epsilon = \frac{8\pi\Phi e^2 \cos\alpha\sqrt{R}}{m^2c^2\omega} p_x$ and modulation frequency $\Omega = \frac{2p_x \cos\alpha}{mc}\omega$. Due to the following two effects ϵ is damped with increasing delay. (i) The electron propagates with p_x during the presence of the IR pulse. The respective change in $\nabla\phi_p(x)$ weakens the energy modulation by e^{-A} with $A = 2\frac{\cos^2\alpha}{(mc)^2}\sigma^2\omega^2 p_x^2$. (ii) The electron propagation during the time between both laser pulses Δt leads to an increase in x where the transient grating intensity recedes [Fig. 1(c)]. This leads to the damping term $e^{-B\Delta t^2}$, $B = \frac{p_x^2 \cos^2\alpha}{2(mc\sigma)^2}$. Since all parameters in Eq. (3) are known, $E_{\mathrm{kin}}(\Delta t)$ has been calculated (solid line, bottom panel of Fig. 2). In addition, Eq. (3) has been fitted to the data for comparison. In Table I we compare the fit result to the analytical values. For R we used our measured value of 0.6. The phase shift ψ is calculated by Fresnel equations.[35] The agreement is remarkable, which proves the explanation of the transient energy variations by acceleration of photoelectrons in the transient grating.

TABLE I. Comparison of theoretical and experimental results for the transient variations of the photoelectron kinetic energy.

	Calculation	Fit
$\epsilon \cdot e^{-A}$	0.82(3) meV	0.81(4) meV
B	$3.7(1) \times 10^{-3}$ ps^{-2}	$3.7(5) \times 10^{-3}$ ps^{-2}
Ω	9.9(4) rad ps^{-1}	9.59(1) rad ps^{-1}
ψ	169°	173(3)°

A value of ψ close to 180° is the consequence of the node of the electric field near the surface. Thus, for the first quarter of the period $\nabla\phi_p$ is directed toward the surface which decelerates the electron (Fig. 2, bottom). To understand that ψ is $<180°$ dissipative processes have to be taken into account. The responding conduction electrons that rearrange to screen the incident electric field experience damping[36] and the node in the electrical field shifts out of the surface as observed in the experiment. However, as we will show in Sec. III, a time independent phase is an oversimplification.

Beside the photoelectron energy we measure the photoemission intensity and an analysis of the intensity allows access to the dispersion of the laser-induced acceleration of photoelectrons with kinetic energy. Figure 3 depicts the transient variation in the photoemission intensity for different initial states and E_{kin} after subtraction of the spectrum with the IR pulse blocked (shown in Fig. 2, top). Figure 4, top, displays the spectra recorded with the used UV photon energies of 4.5 and 6.0 eV while the IR pulse was present. The oscillation amplitude is largest in the vicinity of the surface-state photoemission line and weaker at lower energy. For kinetic energies between 1.0 and 1.5 eV, where the spectrum is almost flat, the weakest variations were observed. Hence, we conclude that the intensity variations are related to the

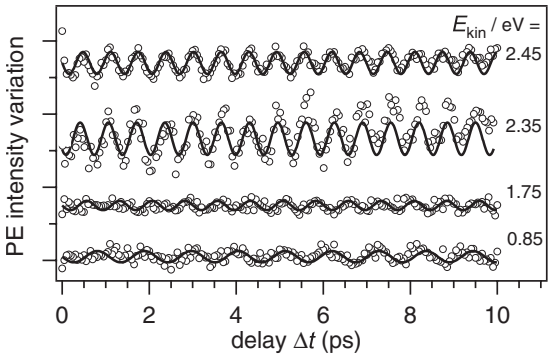

FIG. 3. Time-dependent variation in the photoemission intensity for different kinetic energies as indicated ($h\nu_{UV}=6$ eV). The amplitude variations scale with each other and depend on the gradient of the intensity with kinetic energy. Solid lines represent fits to the data by a sine function.

gradient of the photoemission spectrum with kinetic energy. To analyze the dependence of the oscillating intensities on the electron momentum we extract the frequency of transient changes in intensity by fitting a sine function to the time-dependent intensities. The resulting frequencies are depicted in the bottom panel of Fig. 4. As pointed out above $\Omega = \frac{2\omega \cos \alpha}{mc} p_x$. Thus, Ω is expected to disperse with $\Omega = C\sqrt{E_{kin}}$. We fit a square-root function to the data in Fig. 4 and find $C/2\pi = 0.99(2)$ THz/$\sqrt{\text{eV}}$. This is in good agreement with the calculated value of $C/2\pi = 1.01(4)$ THz/$\sqrt{\text{eV}}$.

At this point we conclude that we understand the process leading to the observed oscillatory behavior in the kinetic energy and photoemission intensity. We proceed by considering the information regarding ultrafast electron dynamics which is encoded in the observed signal. The concept relies on superposition of incoming and reflected fields to the transient grating. An investigation of electron dynamics within one or few optical cycles would certainly benefit from laser pulses with a few optical cycles. Nevertheless, the accessible dynamics is intrinsically independent of the carrier-envelope phase because the grating represents a standing wave and the employed detection averages over the quiver motion $\mathbf{r}_1$. However, the scheme is sensitive to a phase shift between incident and reflected fields because such a phase shift displaces the grating along the surface normal. To access this regime we have carried out calculations using a simplified description of electron transport in the metal which will be presented in Sec. III. These results illustrate the accessible electron dynamics and comprise of a time-dependent phase and amplitude evolution of the reflected light field. Furthermore, our analysis using 50 fs pulses suggests a way to determine the Drude scattering rate Γ.

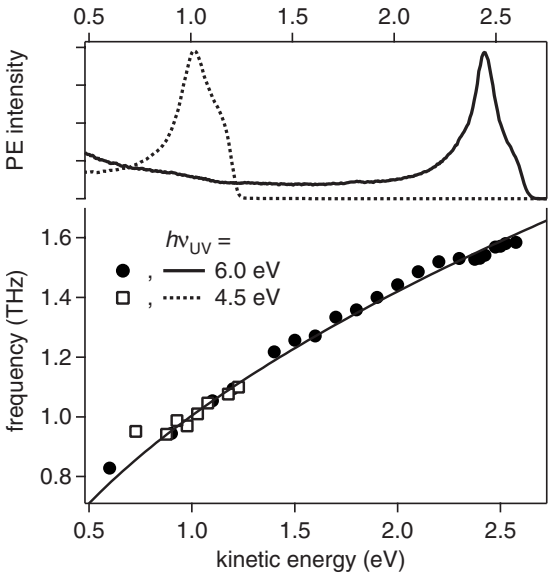

FIG. 4. Top: photoemission spectra at indicated photon energies while the IR pulse is present. The intensity increase recognized for the 6 eV data at low energy was absent in Fig. 2 and is attributed to hot electrons generated by absorption of IR photons. Bottom: dispersion of the oscillation frequency $\Omega/2\pi$ with kinetic energy. The solid line is a fit by a square-root dependence of oscillation frequency on the kinetic energy.

III. TRANSPORT THEORY DESCRIPTION

In the above description a difference in envelope amplitude and a constant phase shift between the incident and reflected IR fields was included. As we will show below this is a severe limitation and does not account for all expected dynamics. In the following we will include the conduction-electron response of the metal explicitly. The reflected light field $\mathbf{E}_2(\mathbf{r},t)$ is generated by the response of the conduction electrons to the incident light field $\mathbf{E}_1(\mathbf{r},t)$. Following Eq. (2) the momentum change is in this case given by

$$\Delta \mathbf{p} = \sum_{i,j=1}^{2} \int_{-\infty}^{\infty} dt \mathbf{F}_{ij} = \frac{q^2}{m^2\omega^2} \int_{-\infty}^{\infty} dt \nabla_{\mathbf{r}=\mathbf{r}_0} \mathbf{E}_1(\mathbf{r},t)\mathbf{E}_2(\mathbf{r},t), \tag{4}$$

with $\mathbf{F}_{12}(\mathbf{F}_{21})$ as the ponderomotive force leading to acceleration in the direction of the gradient of the reflected (incident) field. The components $\mathbf{F}_{11}(\mathbf{F}_{22})$ do not contribute because no grating will be generated by the incident (reflected) field alone. The incident field, chosen for the following calculation, reads

$$\mathbf{E}_1(\mathbf{r},\alpha,t) = E_0 \mathbf{n}_1 \sin[\omega(t-\Delta t^*)] e^{-|t-\Delta t^*|/\tau} \tag{5}$$

with the field amplitude E_0 and the polarization vector $\mathbf{n}_1$; $\Delta t^* = \Delta t \beta \cos \alpha$ is a scaled time delay with $\beta m = p_x/c$. We understand that this is a rather unrealistic pulse shape. We use it nevertheless for these illustrative considerations to perform an analytical calculation, which is inhibited for field pulses with a more realistic Gaussian or hyperbolic secant envelope. We assume that the specific shape is of minor importance because the laser field is smoothed by the above integration. The reflected field from the metal surface is determined by a simplified transport equation for electrons in a single band model that describes the metal and includes a typical drift term induced by the applied IR field $\mathbf{E}$ and a relaxation term proportional to Γ,

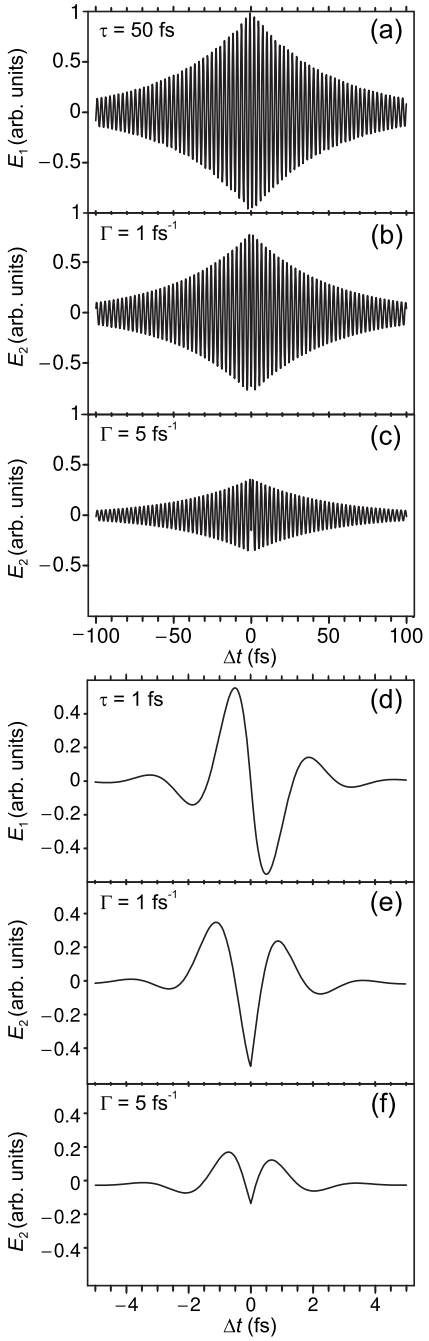

FIG. 5. [(a) and (d)] Incident fields with pulse duration τ of (a) 50 and (d) 1 fs. Respective reflected fields are given for [(b) and (e)] $\Gamma=1$ fs^{-1} and [(c) and (f)] $\Gamma=5$ fs^{-1}.

$$\left(\partial_t + \frac{-e\mathbf{E}(\mathbf{r},t)}{\hbar}\cdot\nabla_{\mathbf{k}}\right) f_{11,\mathbf{k}} = -\Gamma(f_{11,\mathbf{k}} - f^0_{11,\mathbf{k}}), \tag{6}$$

with $f^0_{11,\mathbf{k}}$ being the initial equilibrium Fermi distribution before the pulse. Equation (6) is solved by a power-series approach for $f_{11,\mathbf{k}}$. The result scales with the electric field $f_{11,\mathbf{k}}=\Sigma_n E^n f^{(n)}_{11,\mathbf{k}}$ up to the first order (linear optics) and is transformed into the frequency domain, where the induced current density $\mathbf{j}$ within the metal is calculated. Using Eq. (5), the reflected field $\mathbf{E}_2(\mathbf{r},\alpha,\omega)=-\frac{1}{2\pi\epsilon_0 c}\mathbf{j}(\mathbf{r},\alpha,\omega)$ and transforming the reflected field from frequency domain back into time domain we find[37]

$$\begin{aligned}
&\mathbf{E}_2(\Delta t^*,t)/C \\
&= \Theta(t-\Delta t^*)\left\{\frac{\tau-\Gamma\tau^2}{(1-\tau\Gamma)^2+\omega^2\tau^2}\sin[\omega(t-\Delta t^*)]\cdot e^{-(t-\Delta t^*)/\tau}\right. \\
&\quad + \frac{\omega\tau^2}{(1-\tau\Gamma)^2+\omega^2\tau^2}\cos[\omega(t-\Delta t^*)]\cdot e^{-(t-\Delta t^*)/\tau} \\
&\quad \left. - \left[\frac{\omega\tau^2}{(1-\tau\Gamma)^2+\omega^2\tau^2} - \frac{\omega\tau^2}{(1+\tau\Gamma)^2+\omega^2\tau^2}\right]\cdot e^{-\Gamma(t-\Delta t^*)}\right\} \\
&\quad + \Theta(\Delta t^*-t)e^{-(\Delta t^*-t)/\tau}\left\{\frac{\tau+\Gamma\tau^2}{(1+\tau\Gamma)^2+\omega^2\tau^2}\right. \\
&\quad \left.\times\sin[\omega(t-\Delta t^*)] + \frac{\omega\tau^2}{(1+\tau\Gamma)^2+\omega^2\tau^2}\cos[\omega(t-\Delta t^*)]\right\}
\end{aligned} \tag{7}$$

with $C=\frac{2\pi^2}{c}E_0\omega_{\mathrm{pl}}\sin\alpha$ and $\omega_{\mathrm{pl}}=\frac{q^2 n_{\mathrm{el}}}{\epsilon_0 m^*}$ (m^* effective mass) as the plasma frequency. Figure 5 shows incident and reflected fields for two pulse durations $\tau=1$ and 50 fs and two scattering rates $\Gamma=1$ and 5 fs^{-1}. For $\tau=50$ fs we have $\tau\Gamma\gg 1$ and memory effects such as plasmon formation can be neglected. The reflected and incident fields are identical except of the phase jump expected by reflection on metal surfaces and a change in amplitude due to a reflectivity below unity. For $\tau=1$ fs we are in the limit of $\tau\Gamma\sim 1$ and memory effects should come into play. The reflected fields are for both evaluated Γ asymmetric with respect to $t=0$.

We proceed and calculate the experimental observable. The momentum change in the photoelectron Δp_x as a function of the time delay Δt (or Δt^*) within the transient grating is caused by the interference of the incident and reflected fields described by Eqs. (5) and (7), respectively,

$$\Delta p_x = De^{-2\Gamma\Delta t^*}\times\frac{128\omega^2\Gamma^3\tau^6}{N^{+2}N^{-2}} \tag{8}$$

$$\begin{aligned}
&+ De^{-2\Delta t^*/\tau}\times\frac{8\Delta t^*}{N^-}[(1-\Gamma\tau+\omega^2\tau^2)\cos 2\omega\Delta t^* \\
&- \omega\Gamma\tau^2\sin 2\omega\Delta t^*]
\end{aligned} \tag{9}$$

$$\begin{aligned}
&+ De^{-2\Delta t^*/\tau}\times\frac{4}{N^-}\left\{\left[\omega\tau^2(1+\Gamma\tau) - \frac{1-\Gamma\tau}{\omega}\right]\right. \\
&\times\sin 2\omega\Delta t^* + \frac{8\omega^2\Gamma^2\tau^5}{N^+N^-}(\sin 2\omega_L B - \cos 2\omega_L B) \\
&\left. - \frac{4\omega\Gamma\tau^3[(1-\Gamma^2\tau^2)-2\omega^2\Gamma\tau^3]}{N^+N^-}\sin 2\omega\Delta t^*\right\}
\end{aligned} \tag{10}$$

$$\begin{aligned}
&= E\times e^{-2\Gamma\Delta t^*} + e^{-2\Delta t^*/\tau}[c_1(\Delta t^*) \\
&\times\cos(2\omega\Delta t^*) + c_2(\Delta t^*)\times\sin(2\omega\Delta t^*)]
\end{aligned} \tag{11}$$

with $D=-\frac{2\pi^2 E_0^2\sin^2\alpha e^2\omega_{\mathrm{pl}}}{m^2\omega^2 c}$ and $N^{\pm}=(1\pm\Gamma\tau)^2+\omega^2\tau^2$. Equation (8) shows a signal decay with $(2\Gamma\beta\cos\alpha)^{-1}$; Eqs. (9) and

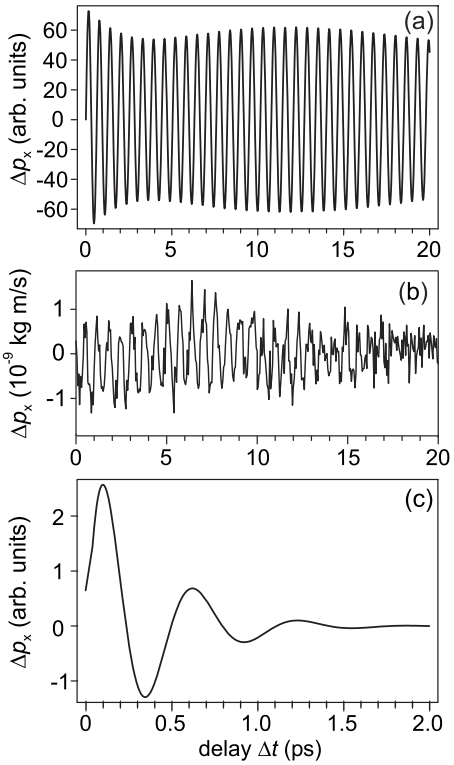

FIG. 6. [(a) and (c)] Calculated and (b) measured change in the electron momentum along the surface normal as a function of pump-probe delay, i.e., distance from the surface (cf. Fig. 2). Parameters of the calculation are $\omega=2.3$ fs^{-1} and $\Gamma=1$ fs^{-1}. The pulse durations are chosen as 50 and 1 fs for panels (a) and (c), respectively. The measured momentum change depicted in panel (b) is based on the data shown in Fig. 2. The kinetic-energy modulation is converted into the momentum change using $\Delta p_x=\Delta E_{\mathrm{kin}}\sqrt{\frac{m}{2E_{\mathrm{kin}}}}$ with $E_{\mathrm{kin}}=2.4464$ eV.

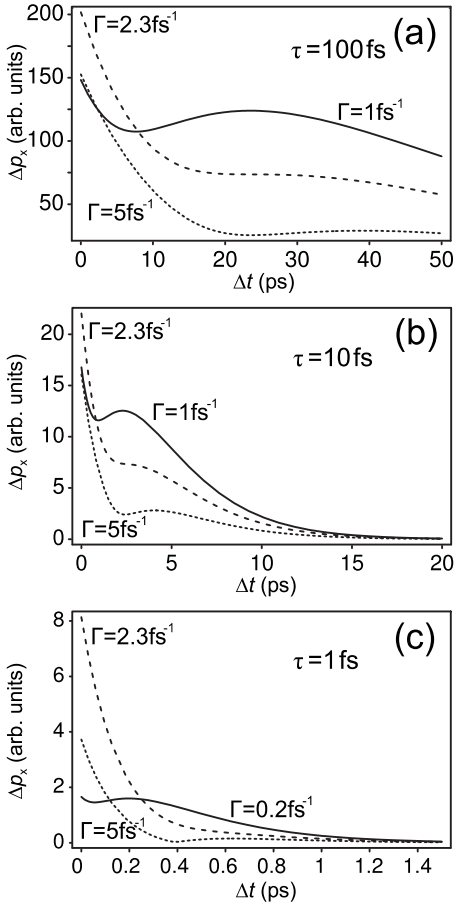

FIG. 7. Plots of the envelope function of Δp_x as a function time delay for different pulse durations of the incident field τ and scattering rates Γ as indicated. Note the different scalings of panels (a)–(c).

(10) show sinusoidal and cosinusoidal oscillations with a frequency $2\omega\beta\cos\alpha$, which is not affected by the values of τ and Γ. Their decay occurs with $(\frac{2\beta\cos\alpha}{\tau})^{-1}$, while Eq. (9) additionally scales with $\beta\cos\alpha\Delta t$. Figure 6 shows exemplary results of Eq. (11) for a typical scattering rate of $\Gamma=1$ fs^{-1} and the laser frequency $\omega=2.3$ fs^{-1}. Panels (a) and (c) depict the calculated behavior for a pulse duration $\tau=50$ and 1 fs, respectively. For larger pulse durations such as 50 fs where $2\pi/\tau \ll \omega$ the momentum change exhibits a minimum and a maximum as a function of Γ. For small pulse duration with $2\pi/\tau \sim \omega$ [Fig. 6(c)] this is not visible because of the pronounced damping of the signal, which depends on the pulse duration.

The encountered extremal values in the envelope of the momentum change as a function of Γ suggest a more detailed investigation. The envelope function of the momentum change can be determined from Eq. (11), which can be written as

$$\Delta p_x \sim E \times e^{-2\Gamma\Delta t^*} + \sqrt{c_1^2(\Delta t^*)+c_2^2(\Delta t^*)}e^{-2\Delta t^*/\tau}\cos[2\omega\Delta t^* + \alpha(\Delta t^*)] \quad (12)$$

with $\tan\alpha(\Delta t^*)=-\frac{c_2(\Delta t^*)}{c_1(\Delta t^*)}$ as a time-dependent phase. The first term is negligible for all combinations of the parameters τ and Γ because either the coefficient E or the exponential function $e^{-2\Gamma\Delta t^*}$ is of negligible order. Neglecting the first term the envelope function is $\sqrt{c_1^2(\Delta t^*)+c_2^2(\Delta t^*)}e^{-2\Delta t^*/\tau}$. Figure 7 shows the envelope function for different values of τ and Γ. With increasing Γ the position of the extremal value of the envelope function shifts to the earlier delays, i.e., closer to the surface, which facilitates a determination of Γ from experimental data as explained in the following. Figure 8 shows the real part of the time delay exhibiting minima (solid) and maxima (dashed) in the envelope function as a function of Γ. There are two areas with minima and maxima in the envelope connected by a line. The time delay interval of this connecting line is complex which results in a saddle point (cf. dashed curves in Fig. 7). For smaller Γ and fixed τ the extremal values are shifted to smaller time delay. The same behavior is observed for constant Γ and smaller τ. As it is clearly visible in Fig. 7, the faster the momentum change decays, the shorter the laser pulse is, which is explained by the fact that the transient grating extends less into vacuum for shorter pulses. Note that the drift velocity of the photoelectron is $3\times10^{-3}c$ and thus the photoelectron essentially remains at its position while the transient grating is formed and decays.

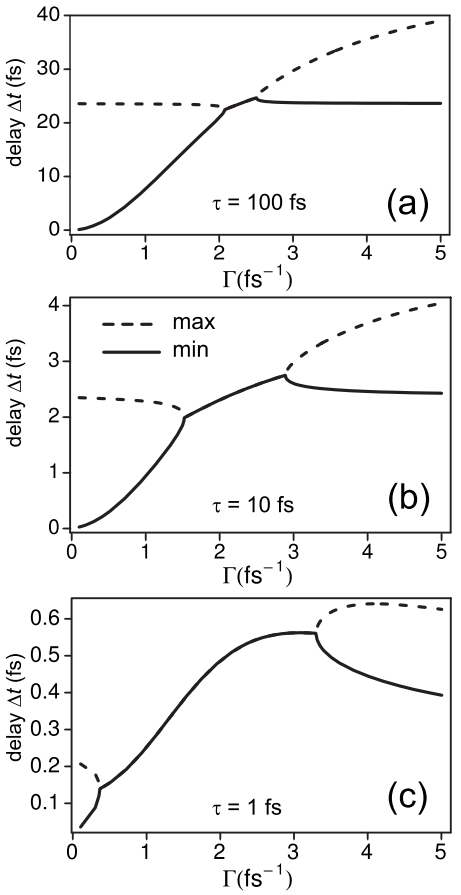

FIG. 8. Plots of the envelope function of Δp_x as a function of time delay and scattering rate Γ. On the connection line between the two bifurcations—left and right—the momentum change presents only saddle points. The solid line describes the position of the minimum and the dashed line is the position of maximum momentum change. Panels (a)–(c) describe the behavior for 100, 10, and 1 fs pulse duration, respectively.

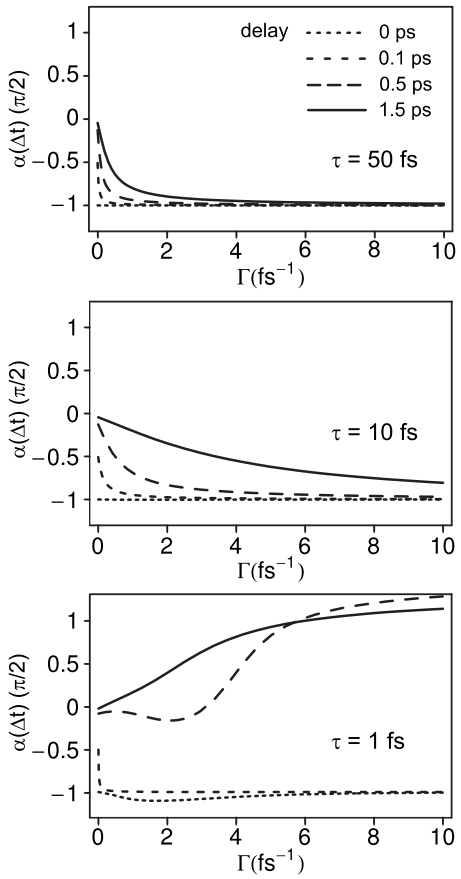

FIG. 9. Dependence of the phase $\alpha(\Delta t)$ in units of $\pi/2$ as a function of Γ in fs^{-1} for different pulse durations τ and time delay Δt as indicated.

Based on these considerations we propose the following method to determine Γ from the momentum change in the photoelectron. After measuring the momentum change the position of the minima and maxima of the envelope is determined. Keeping τ constant determines the parameter space $(\Delta t, \Gamma)$ of minima and maxima for the respective pulse duration which is determined independently (Fig. 8). The experimentally determined delays of minimum and maximum can then be assigned to a unique relaxation rate Γ that describes the investigated system. Suppose no extremal values are found, then the value of Γ lies in the interval of the connection line. Figure 8 illustrates that the extend of the connection line decreases with increasing pulse duration and a measurement with larger τ will deliver two possibilities. First, minima and maxima appear. In this case Γ can be determined as outlined above. Second, no minima and maxima are identified. Then one will get at least a small range for Γ giving a reasonable approximation for the relaxation rate.

The shift of the maximum (minimum) can be explained with the grating itself. Extrapolating the maximum position for small Γ to the minimum position for large Γ shows that the actual time delay is identical, but the minimum turns into a maximum [see Fig. 8(a)]. Since Γ is identical for these low and high limits, i.e., the metal conduction electrons do not influence this momentum change, we conclude that this limit is determined by acceleration of photoelectrons along the gradient of the *incident* field. In turn, the minimum for small and the maximum for large Γ that do exhibit different time delays are the result of photoelectron acceleration along the field gradient of the *reflected* field which is modified by the relaxation rate of the electrons in the surface. The Γ interval of the connection line between the bifurcations, which shows no extremal values, describes the regime where acceleration and deceleration along the field gradient of the incident and reflected fields cancel each other. In this case, only a decay of the ponderomotive signal is encountered for all time delays.

Finally, we report on the evolution of the phase α defined in Eq. (12) as a function of time delay. We encounter pronounced effects which are presented in Fig. 9. The phase of the detected momentum change is directly related to the phase change in the reflected light field with respect to the incoming one. The time dependence of α demonstrates that the phase of the reflected light field takes considerable time to arrive at the equilibrium limit described by conventional metal optics in the frequency domain. With increasing Γ and a nonzero delay the asymptotic limit of $-\pi/2$ is reached for

large Γ except for the case of short pulses $\tau=1$ fs. This finding illustrates that at large Γ the conduction-band electrons respond quickly enough in relation to the duration of an optical cycle leading to a value of α close to $\pi/2$. On the other hand, the deviations from this ideal value are pronounced for small Γ and transient effects have to be taken into account before a continuous-wave response is established. The different panels in Fig. 9 show the behavior for different laser-pulse durations τ. It is obvious that τ has a strong influence on $\alpha(\Gamma,\Delta t)$. The effects can be understood qualitatively as follows. A rather long laser pulse consists of many optical cycles and the conduction electrons have enough time to tune into the light field frequency. For shorter pulse this becomes more difficult as the pulse consists of less cycles and the amplitudes of consecutive optical pulses change. In the limit of the 1 fs pulse, depicted in Fig. 9, bottom panel, this even leads to another asymptotic value of $\pi/2$. A pulse duration of 1 fs for an 800 nm pulse might appear artificial. However, the result nicely illustrates the importance of such effects, as the asymptotic value is changed.

Thereby we have established that in case of a reflection of an ultrashort electromagnetic field pulse, it is not sufficient to know the electronic response function and laser frequency alone, as we have assumed in Sec. II. In fact, the laser field itself has to be taken into account to find the correct response function of the metal. Collective electronic excitations driven by the laser field have to be taken into account and memory effects certainly cannot be neglected.

IV. DISCUSSION

A direct comparison of the theoretical and experimental findings regarding the momentum change imposed on the photoelectron by the ponderomotive potential of the transient grating is given in Figs. 6(a) and 6(b). Albeit we have detected and explained the periodic acceleration of the photoelectron, the essential feature of extremal values in the envelope of momentum change has not yet been observed in the experiment. From the theoretical side future efforts are to include the effects of the frequency dependence of Γ, which were not included in our present approach. This would become essential if future experiments using more intense or shorter pulses leading to nonlinear excitation find deviations compared to the present theoretical description.

A closer look to the experimental results suggests that fluctuations in the signal, which are actually below 1 meV (Fig. 2), might be responsible for not finding minima and maxima in the envelope. In the following we discuss how this problem can be overcome and the full capability of the method demonstrated by the transport theory description can be achieved.

We consider two pathways to improve the experimental sensitivity. We have analyzed if an optimum parameter set exists to detect minima and maxima in the envelope function [Eq. (12)]. Without going into details, we note that a large time delay between minimum and maximum and a high contrast in the minimum and maximum momentum change are beneficial for their detection. An analysis of the variation in τ and Γ shows that it is reasonable to start experiments with 800 nm laser pulses for transition metals with scattering rates of several 1 fs^{-1}. For noble metals with higher scattering rates the delay between minimum and maximum is reduced and might become unfavorable for a detection of extremal values in Δp_x.

An increase in the gradient of the ponderomotive potential will lead to larger momentum changes and might reduce problems related to fluctuations in the analysis of the photoelectron's kinetic energy. This could be realized by performing the experiment using more energetic laser pulses. Typically 1–10 kHz Ti:sapphire amplifiers deliver 800 nm pulses with peak intensities of about 100 TW/cm^2, which will increase the acceleration of the photoelectron compared to the presented setup up to 3 orders of magnitude (current peak intensities are 50 GW/cm^2). This might well compensate the reduction in laser repetition rate by a factor of 10–100. Experiments by Miaja-Avila *et al.*[25] already demonstrated the capability of time-resolved photoemission techniques using kilohertz amplifiers in above threshold ionization studies from metal surfaces.

Regarding the question of the optimal pulse duration we point out that the advantage of shorter pulses is that the signal can be increased compared to longer pulses. Therefore, the position of minimum and maximum can be detected with better accuracy. However, a pulse width of a few optical does not necessarily provide improved results for the proposed method since an important part of the experiment is the optical grating formed by self-interference of the optical pulse. For too short pulses, the grating is not stable for a sufficient time to interact with the moving electrons. Therefore, an optimal pulse length takes both increased signal and sufficient light-electron interaction into account.

V. CONCLUSION

In summary, we have analyzed the interaction of a standing electromagnetic wave with electrons by femtosecond time-resolved photoemission from a metal surface. We present evidence for acceleration of photoelectrons in the spatial gradient of the ponderomotive potential in free space. The analysis is based on (i) transient kinetic-energy (or momentum) variations in electrons photoemitted from the Gd(0001) surface state and on (ii) transient changes in the photoemission intensity. An analytical description of the electric field of the transient grating is in good agreement with the experiment. Thus, the demonstrated technique facilitates an analysis of the transient optical grating. If the incident light field is known, the reflected light field, which contains information of collective electron dynamics such as plasmon excitation/decay and the buildup of screening the IR field, can be extracted. Using a simplified transport theory we calculate the expected momentum change in a linear limit and reveal an envelope function of the photoelectron's periodic acceleration in the transient grating, which allows us to separate effects of the incoming and the reflected field contributions. The phase of the detected periodic momentum change represents an interesting quantity. Albeit not yet experimentally verified, it presents a temporal evolution that is

directly related to the phase of the collective excitation of the metal conduction electrons. Our results establish that the phase is dependent on the duration of the incoming laser pulse, which can only be understood, if memory effects are taken into account.

ACKNOWLEDGMENTS

We thank S. Butscher for fruitful discussions and acknowledge funding by the Deutsche Forschungsgemeinschaft through SPP 1133 and CoE Unicat.

*uwe.bovensiepen@fu-berlin.de

†Present address: Femtolasers Production GmbH, Fernkorngasse 10, 1100 Vienna, Austria.

‡Present address: Foundation for Research and Technology-Hellas, Institute of Electronic Structure and Laser, N. Plastira, P.O. Box 1385, Vassilika Vouton, Heraklion 71110, Greece.

[1] M. Lindberg and S. W. Koch, Phys. Rev. B **38**, 3342 (1988).

[2] R. Binder, S. W. Koch, M. Lindberg, W. Schäfer, and F. Jahnke, Phys. Rev. B **43**, 6520 (1991).

[3] E. T. J. Nibbering, D. A. Wiersma, and K. Duppen, Phys. Rev. Lett. **66**, 2464 (1991).

[4] P. Hamm, M. Lim, and R. M. Hochstrasser, Phys. Rev. Lett. **81**, 5326 (1998).

[5] M. Richter, T. Renger, and A. Knorr, Photosynth. Res. **95**, 119 (2008).

[6] T. Shih, K. Reimann, M. Woerner, T. Elsaesser, I. Waldmüller, A. Knorr, R. Hey, and K. H. Ploog, Phys. Rev. B **72**, 195338 (2005).

[7] F. J. Rodriguez, L. Quiroga, C. Tejedor, M. D. Martin, L. Vina, and R. Andre, Phys. Rev. B **78**, 035312 (2008).

[8] W. Hoyer, A. Knorr, J. V. Moloney, E. M. Wright, M. Kira, and S. W. Koch, Phys. Rev. Lett. **94**, 115004 (2005).

[9] M. Richter, M. Schaarschmidt, A. Knorr, W. Hoyer, J. V. Moloney, E. M. Wright, M. Kira, and S. W. Koch, Phys. Rev. A **71**, 053819 (2005).

[10] Y. Kurzweil and R. Baer, Phys. Rev. B **73**, 075413 (2006).

[11] M. L. Cowan, B. D. Bruner, N. Huse, J. R. Dwyer, B. Chugh, E. T. J. Nibbering, T. Elsaesser, and R. J. D. Miller, Nature (London) **434**, 199 (2005).

[12] C. Voelkmann, M. Reichelt, T. Meier, S. W. Koch, and U. Höfer, Phys. Rev. Lett. **92**, 127405 (2004).

[13] H. Petek and S. Ogawa, Prog. Surf. Sci. **56**, 239 (1997).

[14] U. Höfer, I. L. Shumay, C. Reuß, U. Thomann, W. Wallauer, and T. Fauster, Science **277**, 1480 (1997).

[15] J. Güdde, M. Rohleder, T. Meier, S. W. Koch, and U. Höfer, Science **318**, 1287 (2007).

[16] A. Kubo, N. Pontius, and H. Petek, Nano Lett. **7**, 470 (2007).

[17] D. J. Bergman and M. I. Stockman, Phys. Rev. Lett. **90**, 027402 (2003).

[18] M. Drescher, M. Hentschel, R. Kienberger, G. Tempea, C. Spielmann, G. A. Reider, P. B. Corkum, and F. Krausz, Science **291**, 1923 (2001).

[19] M. Drescher, M. Hentschel, R. Kienberger, M. Uiberacker, V. Yakovlev, D. Scrinzi, T. Westerwalbesloh, U. Kleineberg, U. Heinzmann, and F. Krausz, Nature (London) **419**, 803 (2002).

[20] E. Goulielmakis, M. Uiberacker, R. Kienberger, A. Baltuska, V. Yakovlev, A. Scrinzi, Th. Westerwalbesloh, U. Kleineberg, U. Heinzmann, M. Drescher, and F. Krausz, Science **305**, 1267 (2004).

[21] A. L. Cavalieri *et al.*, Nature (London) **449**, 1029 (2007).

[22] H. G. Muller, P. Agostini, and G. Petite, *Atoms in Intense Laser Fields*, Advances in Atomic, Molecular, and Optical Physics Suppl. 1 (Academic, New York, 1992).

[23] S. E. Irvine, A. Dechant, and A. Y. Elezzabi, Phys. Rev. Lett. **93**, 184801 (2004).

[24] F. Bisio, M. Nývlt, J. Franta, H. Petek, and J. Kirschner, Phys. Rev. Lett. **96**, 087601 (2006).

[25] L. Miaja-Avila, C. Lei, M. Aeschlimann, J. L. Gland, M. M. Murnane, H. C. Kapteyn, and G. Saathoff, Phys. Rev. Lett. **97**, 113604 (2006).

[26] J. M. Schins, P. Breger, P. Agostini, R. C. Constantinescu, H. G. Muller, G. Grillon, A. Antonetti, and A. Mysyrowicz, Phys. Rev. Lett. **73**, 2180 (1994).

[27] T. E. Glover, R. W. Schoenlein, A. H. Chin, and C. V. Shank, Phys. Rev. Lett. **76**, 2468 (1996).

[28] G. Schmidt, *Physics of High Temperature Plasmas* (Academic, New York, 1979).

[29] A. Melnikov, I. Radu, U. Bovensiepen, O. Krupin, K. Starke, E. Matthias, and M. Wolf, Phys. Rev. Lett. **91**, 227403 (2003).

[30] K. Maiti, M. C. Malagoli, E. Magnano, A. Dallmeyer, and C. Carbone, Phys. Rev. Lett. **86**, 2846 (2001).

[31] A. Rehbein, D. Wegner, G. Kaindl, and A. Bauer, Phys. Rev. B **67**, 033403 (2003).

[32] M. Lisowski, P. A. Loukakos, A. Melnikov, I. Radu, L. Ungureanu, M. Wolf, and U. Bovensiepen, Phys. Rev. Lett. **95**, 137402 (2005).

[33] P. A. Loukakos, M. Lisowski, G. Bihlmayer, S. Blügel, M. Wolf, and U. Bovensiepen, Phys. Rev. Lett. **98**, 097401 (2007).

[34] $e^2 = 1.440$ eV nm (Gauss system).

[35] Optical constants are taken from L. Ward, *Handbook of Optical Constants of Solids* (Academic, San Diego, 1998), Vol. 3. $n = 2.95$ and $k = 3.27$ have been used.

[36] M. Born and E. Wolf, *Principles of Optics* (Pergamon, New York,1975).

[37] T. Stroucken, A. Knorr, P. Thomas, and S. W. Koch, Phys. Rev. B **53**, 2026 (1996).